LBL-14610
Preprint c.2

Lawrence Berkeley Laboratory
UNIVERSITY OF CALIFORNIA

RECEIVED
LAWRENCE
BERKELEY LABORATORY

OCT 4 1982

LIBRARY AND
DOCUMENTS SECTION

To be published as a chapter in COLLECTIVE BANDS IN NUCLEI, Ed. D. Wilkinson, Pergamon Press, Ltd. 1982

COLLECTIVE BANDS IN SOME ROTATIONAL AND TRANSITIONAL NUCLEI

Frank S. Stephens

August 1982

NUCLEAR SCIENCE DIVISION

LBL-14610 c.2

Prepared for the U.S. Department of Energy under Contract DE-AC03-76SF00098

DISCLAIMER

This document was prepared as an account of work sponsored by the United States Government. While this document is believed to contain correct information, neither the United States Government nor any agency thereof, nor the Regents of the University of California, nor any of their employees, makes any warranty, express or implied, or assumes any legal responsibility for the accuracy, completeness, or usefulness of any information, apparatus, product, or process disclosed, or represents that its use would not infringe privately owned rights. Reference herein to any specific commercial product, process, or service by its trade name, trademark, manufacturer, or otherwise, does not necessarily constitute or imply its endorsement, recommendation, or favoring by the United States Government or any agency thereof, or the Regents of the University of California. The views and opinions of authors expressed herein do not necessarily state or reflect those of the United States Government or any agency thereof or the Regents of the University of California.

LBL-14610

Collective Bands in Some Rotational and Transitional Nuclei

Frank S. Stephens

Nuclear Science Division
Lawrence Berkeley Laboratory
University of California
Berkeley, CA 94720

This work was supported by the Director, Office of Energy Research, Division of Nuclear Physics of the Office of High Energy and Nuclear Physics of the U.S. Department of Energy under Contract DE-AC03-76SF00098.

COLLECTIVE BANDS IN SOME ROTATIONAL AND TRANSITIONAL NUCLEI

Frank S. Stephens
Nuclear Science Division, Lawrence Berkeley Laboratory,
University of California, Berkeley, CA 94720

PART 1

ROTATIONAL BANDS IN DEFORMED NUCLEI

INTRODUCTION

The most collective bands known in nuclei are the rotational bands that occur wherever the nuclear shape becomes appreciably nonspherical. Such shapes are due to the shell effects in nuclei. When a shell is filled there is extra stability so that, for the usual (spherical) shell model, a spherical shape is stabilized near closed shells. However, between shells the spherical shape is disfavored and the nucleus deforms in order to find a more favorable energy. Such deformations give rise to an orientation degree of freedom for the nucleus and thereby to the possibility of rotation.

ROTATIONAL PROPERTIES

Energies

A rotational band reflects a very simple type of collective motion, which changes the orientation of the system without essentially affecting its shape or internal structure. The energy associated with the motion is mainly kinetic and may be written

$$E = \frac{1}{2}\mathcal{J}\omega^2 = \frac{\hbar^2}{2\mathcal{J}} I(I + 1) \quad , \tag{1}$$

where the value of $\mathcal{J}$, the moment of inertia, depends on the shape and internal structure, ω is the angular velocity, and I is the angular momentum. This energy relationship expresses one of the most characteristic features of nuclear rotational motion and applies to the rotation of any near-rigid symmetric top. It works even better for diatomic molecules. It is interesting that all the low-lying excitation modes of a nucleus have analogs in a diatomic molecule. Both systems have rotational, vibrational, and particle excitations, with energy scales for the particle excitation (electronic vs. nucleonic) that differ by about 10^6 (eV to MeV). In the molecular case the three modes differ from each other in energy by factors of approximately 50, so they are almost independent (the adiabatic hypothesis works well). However, the (low-lying) nuclear vibrational energies are of the same order as single particle excitations, indicating that this vibrational mode does not become strongly collective in nuclei. The

rotational spacings are only about a factor of 10 smaller than the other two, so that nuclear rotational levels show much larger rotation-vibration and single-particle perturbations than do molecular levels.

Once rotational motion had been suggested by A. Bohr (1) in 1952, it was soon found; following α decay in the actinide nuclei (A ~ 240) and by Coulomb excitation of the lanthanide nuclei (A ~ 160). As a recent example, the γ-ray spectrum of ^{238}U, Coulomb excited by a ^{208}Pb beam (2), is shown in Fig. 1. The level scheme is shown on the right side of Fig. 2, where the first few levels follow the purely rotational motion given by Eq. (1) to a few percent. With increasing spin the deviations become larger as the rotational motion increasingly perturbs the intrinsic structure of the nucleus via the Coriolis and centrifugal interactions. Nevertheless, it is remarkable that such a simple picture works so well over such a large range of spin and excitation energy. Coulomb excitation is also a principal experimental technique for determining the other major characteristic of nuclear rotational bands, namely, the enhancement over single-particle values of the electric quadrupole transition probabilities between rotational levels. This enhancement depends on the magnitude of the electric quadrupole moment, which is related to the amount of deformation. For the strongly deformed lanthanide and actinide nuclei such as ^{238}U shown in Figs. 1 and 2, the enhancement of the rotational transitions is around 200 times the single-particle value.

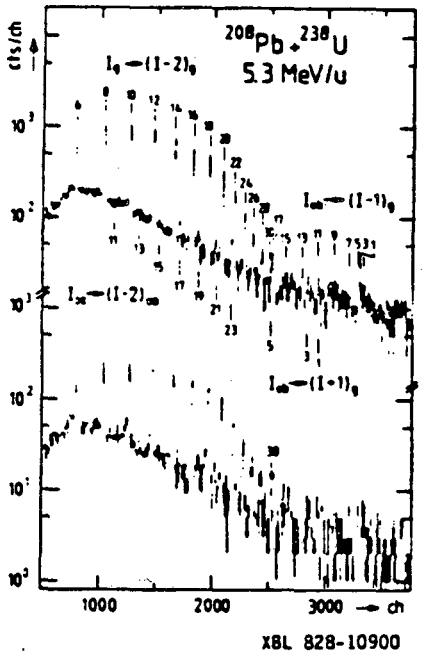

Fig. 1. Doppler corrected gamma spectra from the excitation of ^{238}U (thin target) by ^{208}Pb ions of 5.3 MeV/n scattered into c.m. angles θ between 97° and 146°. Top: gamma spectrum obtained by coincident detection of the scattered projectile and the recoiling target nucleus. Bottom: As top, but requiring an additional coincidence with a second gamma ray Ref. 2).

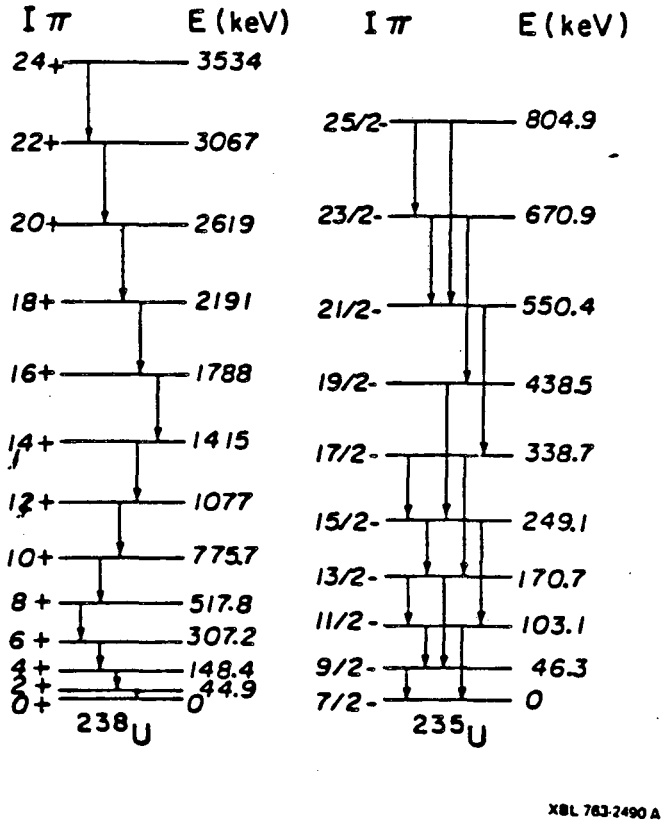

Fig. 2. Level schemes of the ground-state rotational bands of ^{238}U and ^{235}U.

Symmetries

From the observed rotational spectrum, one can deduce many properties of the deformation, in particular its symmetries. For example, Fig. 2 shows that there is only one low-lying band strongly Coulomb excited in ^{238}U, implying approximate axial symmetry. Non-axial nuclei would have more than one band strongly coupled to the ground state, as is discussed in Part 3 of this report. Also, every other spin state is missing, due to a nuclear wave function that is invariant under a 180° rotation of the system at right angles to its symmetry axis (its two ends are the same, like homonuclear diatomic molecules). An important consequence of this is that the emitted radiation, E_γ, is at an energy corresponding to twice the rotational frequency, ω. The presence of an odd nucleon, with a residual angular momentum projection along the symmetry axis, partially lifts this symmetry and every spin value occurs, as is shown by the level scheme for ^{235}U on the left side of Fig. 2. The nuclear wave function is symmetrized so that, although the two ends of the nucleus are still indistinguishable, it may either change sign or not on rotation by 180° at right angles to its symmetry axis. The quantum number α, connected with this symmetry, is called the "signature" and is the only quantum number besides parity that survives at high rotational frequencies. The very large values for the static and transition quadrupole moments indicate that the nuclear deformation is mainly quadrupolar, though there are reasonably large hexadecopole components in many nuclear shapes.

Moment of Inertia

Although many nuclei between closed shells have rotational bands that follow Eq. (1), the moments of inertia are generally not so large as those calculated for a rigid body with the size and mass of the nucleus. They do, however, tend to increase with spin. The value of $\mathcal{J}$ depends both on the shape of the nucleus and the nature of the mass flow during rotation. For structures that are rigid, e.g. simple molecules, all particles take part in the rotation with the same angular velocity. A nucleus is not rigid; the nucleons move throughout the nuclear volume, but so long as the particles move independently, it has been shown (for a harmonic oscillator potential) that the rigid-body moment of inertia results. Nevertheless, the experimental moments of inertia at low spin are smaller than rigid-body values by factors of 2-3. This reduction is due to correlations in the nucleonic motion: the most important ones being due to the pairing interaction. Insofar as two nucleons occupy the exactly time-reversed orbits favored by pairing, they can contribute nothing to the angular momentum (moment of inertia). It is interesting that the pair-correlations in nuclei are almost completely analogous to those in superconductors or superfluids. In fact, the equations of Bardeen, Cooper, and Schriefer (BCS) (3) that first gave an explanation of superconductivity are taken over exactly into the nuclear case and give nearly correctly not only the pairing energy (the energy gap and the odd-even mass difference) but also the reduction in the moment of inertia. The pair correlations, and therefore their effect on the moment of inertia, will be reduced by either an increase in nuclear excitation energy or an increase in nuclear spin. The first reflects a blocking of the levels for the pairs and the second the fact that the Coriolis interaction decouples the oppositely moving members of the pairs. The latter effect might occur suddenly, as it does in superconductors when a critical magnetic field is reached (first order phase transition), or, because the nucleus is a rather small system with only ~100 particles of widely different angular momentum, it might occur gradually. In fact, for nuclei the observed increasing moment of inertia with increasing angular momentum indicates that the decrease of pairing is gradual, though it is not altogether smooth.

Backbending

The lack of smoothness in the changing moment of inertia came as a surprise in 1971 when a discontinuity was found in the energies of the ground state rotational bands of several rare-earth nuclei (4). As the nucleus de-excites from a high initial spin, the regular increase in rotational period (slowing down) is interrupted around spin 14 by a rather sizeable decrease. This corrresponds to an internal rearrangement, a "nuclearquake", and is generally called a "backbend". It is amusing to compare it with another type of quake--a "starquake". Neutron stars or "pulsars" also have regularly increasing periods that occasionally decrease suddenly. The slowing down of the nucleus ^{158}Er is compared with the pulsar Vela in Fig. 3. The behaviors are quite similar, though the percentage

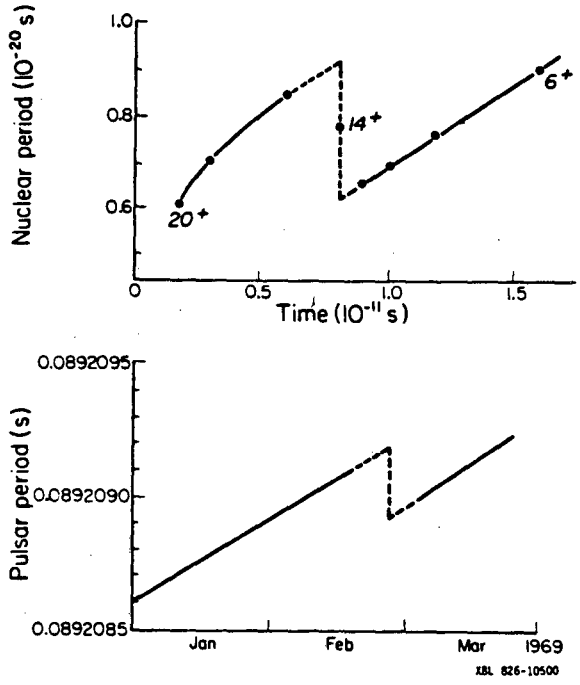

Fig. 3. Plots of rotational period vs time for the nucleus ^{158}Er (top) and the pulsar Vela (bottom).

changes in the nuclear case are much larger. Both ordinate and abscissa differ by about 20 orders of magnitude between these two cases, which indicates that the size of the "glitch" corresponds to the amount of regular change occurring over roughly the same number of periods (~10^8). The pulsar glitches are not too well understood at present but probably have to do with a sudden breaking of the solid crust on the neutron star. The nuclear glitch is much better understood and is due to the sudden pairing of two high-j particles. In the case of this first backbend in ^{158}Er, the particles are $i_{13/2}$ neutrons. Above $I \approx 14$ this pair of aligned particles contributes 10 $\hbar$ along the rotation axis, but this is lost below $I \approx 14$ when the particles suddenly couple to spin nearly zero and begin to participate in the pairing correlations. The angular momentum has to be made up by the collective rotation, which must speed up, thereby decreasing the period.

Such behavior is now well studied in nuclei around ^{158}Er, and the change described above corresponds to a crossing of two rotational bands (5). A band with two aligned $i_{13/2}$ neutrons crosses the ground-state band, which has all particles participating in the pairing correlations (pairing vacuum). Thus the discontinuity actually corresponds to a shift into another band, though the mixing between these bands gives collective enhancement to the transition connecting the bands, often to the point where they are stronger than the "in-band" transitions at the

crossing. The energy of the aligned band relative to the ground band gradually decreases with increasing spin because of the Coriolis interaction. Just as a toy gyroscope will attempt to align its rotation axis with that of its rotating frame, so a pair of high-j particles tends to align its rotation axis (angular momentum) with that of the rotating nucleus, thereby decreasing its energy relative to a band without such alignment. This shift in angular momentum between the orbital motion of individual particles and the collective rotation of the nucleus is illustrated in Fig. 4, where the top figure (b) is the moment of inertia plotted against angular frequency ($\omega = E_\gamma/2$) for the nucleus ^{158}Er. The sharp increases in due to the alignments are apparent: the first one giving rise to a "backbending" as the sequence shifts bands and the second to an "upbend". In the center of Fig. 4, spin is plotted against angular frequency. The members of the three different bands fall rather clearly on separate lines, and the difference in spin between the lines at a given frequency represents the difference in aligned angular momentum, Δi, between the bands at that frequency. This is shown at the bottom of Fig. 4. It is clear that the $(i_{13/2})^2$ band has about 10 aligned relative to the ground band of ^{158}Er. The next higher band has two more particles aligned (4-quasiparticle state), which are believed to be $h_{11/2}$ protons, and the additional Δi is about 7 . Both the spin and the angular frequency in Fig. 4 are directly measurable quantities, another of which is the

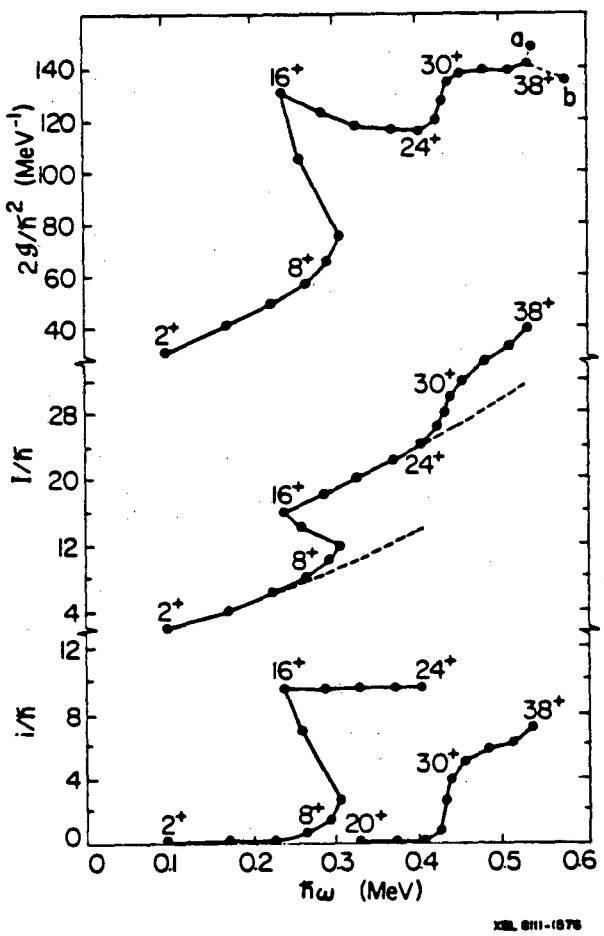

Fig. 4. Plots of the moment of inertia (top), spin (middle), and spin alignment (bottom) vs the rotational frequency for the yrast sequence in ^{148}Er. From ref. 6.

interaction of the two bands as they cross. A strong interaction means heavy mixing of the bands and a "smoothed-out" crossing; whereas weak interactions are associated with sudden sharp crossings. The three quantities, frequency, change in alignment, and interaction strength, (ω, Δi, V), characterize a band crossing, and there is now developing a spectroscopy connected with such crossings. An indication of this new area is given in Fig. 5, which shows the energies of levels of ^{160}Yb plotted against spin (7). In addition to the two band crossings along the yrast sequence, there are many occurring in the bands above.

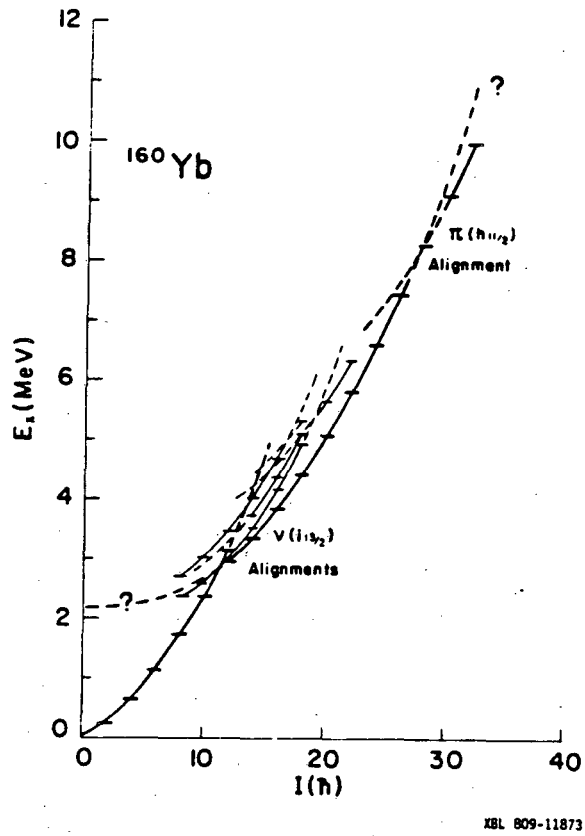

Fig. 5. Rotational band trajectories on an E vs I plot for the levels of ^{160}Yb. The observed levels are indicated by the horizontal marks. From ref. 7.

CALCULATIONS

There is currently much interest in relating these crossings to calculated ones. the deformation requires a modification of the single-particle level spectrum from the usual shell model, in that this spectrum must be calculated in the appropriate nonspherical potential. A number of such calculations have since been made using an anisotropic harmonic-oscillator (Nilsson) potential (8), a Woods-Saxon potential (9), and most recently a Hartree-Fock type approach towards a self-consistent potential (10). These give rather similar results, one of which is shown in Fig. 6. The potential here is the Nilsson one:

$$V = \left[M_3^2\omega_3^2 x + \omega_\perp^2(x_1^2 + x_2^2)\right] + V'_{\ell\ell}\hbar\omega\,(\ell^2 - \langle\ell\rangle_N^2) + V_{\ell s}\hbar\omega_0\,\ell\cdot s \quad , \qquad (2)$$

where M is the nuclear mass, $-V_{\ell\ell} \sim 0.03$ and is added to "flatten" the harmonic oscillator potential, $\langle\ell^2\rangle N = 1/2\ N(N+3)$ keeps the average shell energies unchanged, $-V_{\ell s} \sim 0.13$, and $\hbar\omega_0 \approx 41\ A^{-1/3}$ MeV. The oscillator frequencies can define a deformation, $\delta = 3(\omega_\perp - \ _3)/(2\omega_\perp + \omega_3)$, which is to lowest order $\Delta R/R$ and leads to a nuclear shape,

$$R(\theta) = R_0[1 + \frac{2}{3}\,\delta\,P_2(\cos\theta)], \qquad (3)$$

having quadrupole character with a symmetry axis (3) and a reflection plane (1,2) through the center perpendicular to the symmetry axis. The 2j+1 degeneracy of the spherical shell model orbits is broken, and the resulting levels are characterized by their projection on the symmetry axis, Ω, their signature, α, and their parity, π. They are two-fold degenerate corresponding to time reversal symmetry of the nucleon motion. It is perhaps worth emphasizing that in this fourth oscillator shown in Fig. 6, the $g_{9/2}$ orbit has dropped down into the next lower shell, and the $h_{11/2}$ orbit has intruded from the shell above due to the large spin-orbit

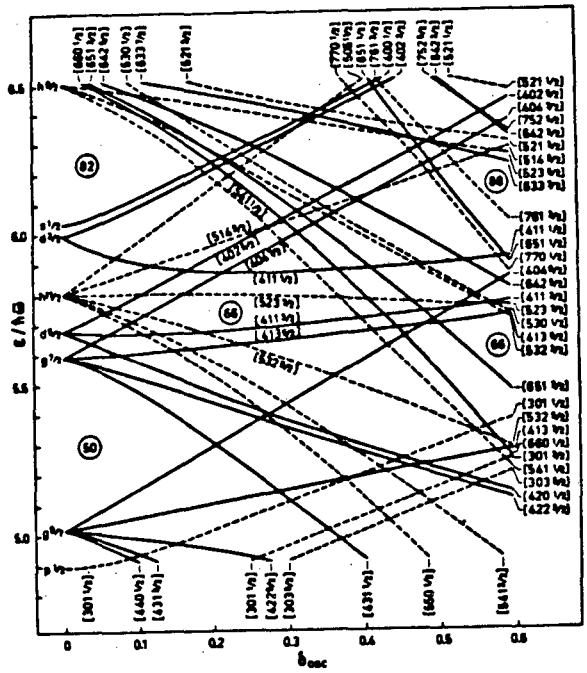

Fig. 6. Energy levels as a function of prolate deformation for protons in the range $50 \leq Z \leq 82$.

splitting. These high-j "intruder" orbits are very important for the high spin states. In general the potentials are not restricted to axial symmetry nor to purely quadrupole shapes. There is a broad spectroscopy based on identifying observed levels with those calculated, and the validity of this kind of approach is now established beyond question.

The next step is to include the rotation. If the problem is simplified to cranking the nuclear potential around the x-axis with a constant frequency ω (the "cranking model"), then the rotation corresponds simply to an additional term, $-\omega j_x$, in the particle Hamiltonian, where j_x is the component of particle angular momentum along the x-axis. This problem has been solved for all the types of potential mentioned previously, and a result (11) for cranking the Nilsson potential for protons (Fig. 5) at a deformation $\epsilon = 0.2$ is shown in Fig. 7. The highest frequencies in Fig. 7 are about the maximum nuclei might acquire before fissioning, but holding the deformation fixed up to this point is not very realistic. There are now available calculations as a function of frequency for a wide variety of shapes, and the energies of the filled levels have been summed for various nucleon numbers, giving the expected shape as a function of frequency. Thus plots like Fig. 7 can now be constructed for the optimum shape parameters at any frequency. Rotation lifts the twofold degeneracy of the orbits associated with time reversal invariance, and mixes the Ω values, so that the remaining quantum numbers are just the parity and signature, π and α, where $\alpha = \pm 1/2$ reflects the remaining symmetry under rotation by 180° around the x-axis. The amount of angular momentum aligned along the x-axis, j_x, for each orbital is proportional to the negative slope, $-d\epsilon/d\omega$, of the lines on Fig. 7, as is apparent from the cranking term in the Hamiltonian, $-\omega j_x$. When the line becomes straight, the alignment is complete (j_x is diagonal). The high alignments acquired by the lowest component of each high-j orbital, e.g., [550 1/2] for $h_{11/2}$ and [660 1/2] for $i_{13/2}$ are apparent.

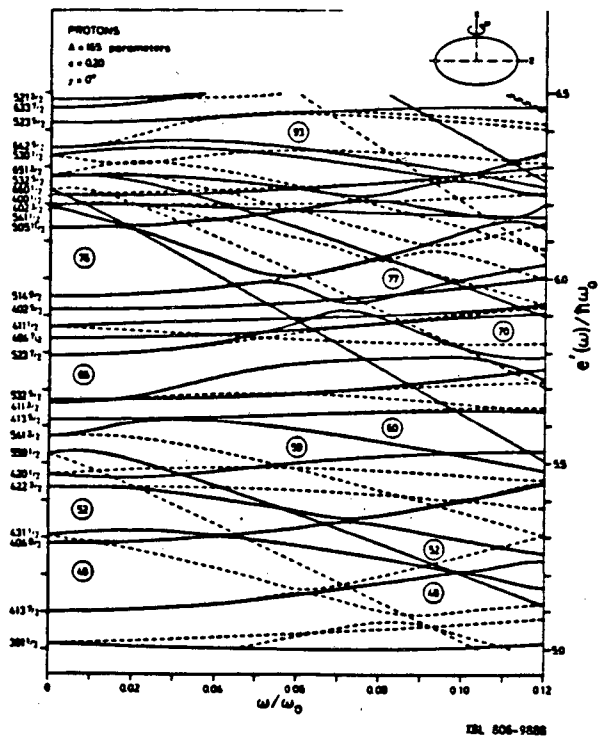

Fig. 7. Energy levels as a function of rotational frequency for protons in a prolate nucleus having $\varepsilon = 0.2$ and mass number 165. The solid and dashed lines correspond to states having different symmetry with respect to $e^{i\pi j_x}$ (different "signatures"). From ref. 11.

The above treatment neglects the pairing correlations, and this is believed to be a good approximation above spins of 30 or 40 $\hbar$, where the correlations are thought to be quenched. However, for lower spins one must solve the cranking calculations with pairing. This can be done either by subsequently solving the BCS equations for a given set of levels (e.g. from Fig. 7) or by adding the pairing into the original diagonalization as in the Hartree-Fock-Bogolyubov method. In either case one gets results (12) like those shown in Fig. 8 for the levels in ^{160}Yb. This diagram covers only a very restricted region, the five states nearest the Fermi level. It is a little complicated to understand Fig. 8; however, it is only at this level that we can appreciate, on the one hand, the underlying single-particle structure of the competition between pairing and rotation and, on the other hand, the current analyses of recent experimental data.

The philosophy for understanding this plot is as follows. The zero-energy line is always the yrast configuration in the even-even nuclei, which is defined to be the "vacuum" of interest. The lines above are then the lowest, second lowest, etc. states having a given set of quantum numbers (α,π). Thus A is the first (+,+) excited state, B the first (-,+) state, E the first (+,-) state, C the second (+,+) state, etc. The configuration along any given line is not fixed, and we use "A", "B", etc. to refer to the initial configurations, and A,B etc. to refer to the lines in Fig. 8. In the frequency range $0 \leq \hbar\omega \leq \hbar\omega_1$, the ground state band, the fully paired quasiparticle vacuum, lies at zero energy (yrast). As the frequency increases in this range, the various excited levels change in energy relative to the ground state, and in particular, "A" and "B" (the aligning $i_{13/2}$ neutron states) fall most steeply (the slope is still proportional to the aligned angular momentum). At frequency $\hbar\omega_1$, the two-quasiparticle state "AB" crosses the ground state and becomes yrast, implying that the curves in Fig. 8 change character; above $\hbar\omega_1$, the energies are measured relative to "AB". Thus a

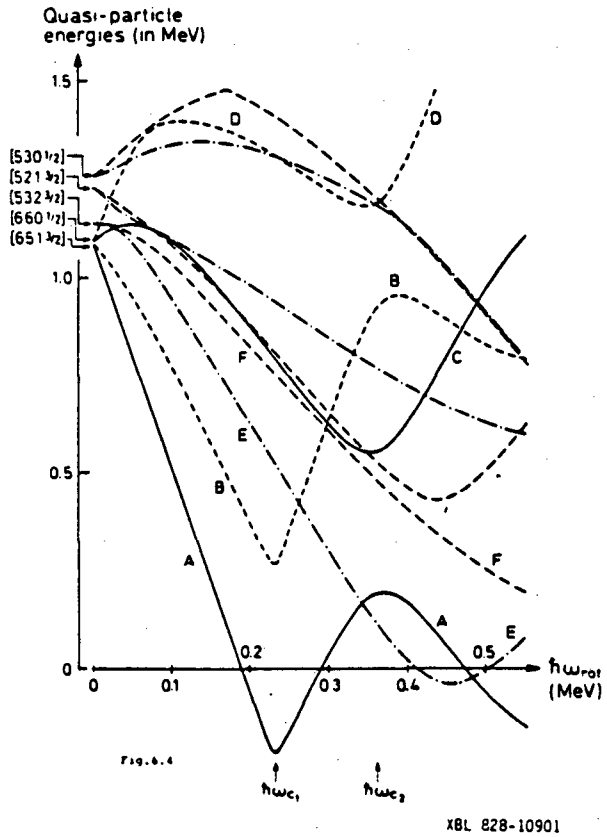

Fig. 8. Quasiparticle spectra for neutrons as a function of rotational frequency, which are calculated from a cranked modified-oscillator model for the fixed parameters suitable for the low-lying states of ^{160}Yb. The quasiparticle orbits with the quantum numbers, $(\alpha=+,\pi=+)$, $(\alpha=-,\pi=+)$, $(\alpha=+,\pi=-)$, and $(\alpha=-,\pi=-)$, are denoted by solid lines, short-dashed lines, dash-dotted lines, and long-dashed, respectively.

nucleus originally in any configuration "X" (not involving "A" or "B") will cross over smoothly at $\hbar\omega_1$ into the state "ABX", having two unpaired and aligned $i_{13/2}$ quasineutrons, i.e., there will be a band crossing in this configuration. This prediction of alignments in many bands at a given frequency will be very important in studies of the highest spin states. The states A and B (or more complicated ones involving "A" or "B") have this crossing blocked, and they do not change configuration at $\hbar\omega_1$. Therefore their energies change slope, reflecting the new "vacuum" (or reference) configuration. States with the same quantum numbers (α,π) cannot actually cross on Fig. 8 so that at $\hbar\omega_2$ the state A (configuration still "A") undergoes a virtual crossing with the state C (configuration "ABC" above $\hbar\omega_1$). The same thing occurs for state B and D at about this same frequency. Since the pairing correlations cannot make use of the two aligned particles above $\hbar\omega_1$, the correlations are diminished, as is the pairing gap. This breaking of one or a few pairs of particles while the pairing correlations still exist for the remaining pairs is a process analogous to that of gapless superconductivity, where the aligned particles play the role of the dilute impurities in the superconductor.

THE NEW SPECTROSCOPY

In order to observe such behavior, the spin range of $I \approx 10$ to $I \approx 30$ for many nuclei in the mass region 100-190 is under intensive spectroscopic study, and a rather detailed picture is emerging. The frequency of a particular crossing (e.g. "AB"--quasiparticle vacuum) depends on several quantities: the pairing gap, the quasiparticle energies, the shape, the residual interactions between quasiparticles, etc. These quantities may be studied as a function of nucleus and configuration by measuring systematically a particular crossing frequency in

different nuclei and bands. So far, this method has been used to measure the pairing gap, Δ, and the effect on it of adding a quasiparticle (blocking a state). This kind of analysis has so far been made only by Garrett and colleagues (13) in Copenhagen. The bottom part (a) in Fig. 9 shows the crossing frequency measured in various odd-A nuclei and their even-even neighbors in the central rare-earth region. The odd-A nuclei have lower crossing frequencies due to a smaller pairing gap (blocking effect). Figure 10 illustrates why this is the

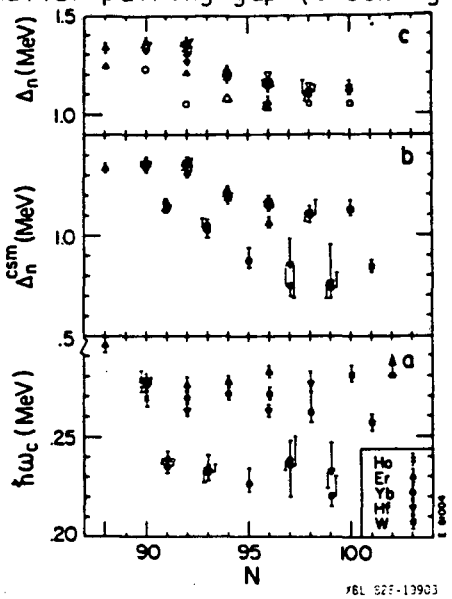

Fig. 9. a) Systematics of the frequency of the lowest frequency bandcrossing, $\hbar\omega_c$, for yrast bands in even-N nuclei and for the lowest negative-parity band in odd-N nuclei. b) Values of Δ_n^{csm} necessary to reproduce the value of $\hbar\omega_c$, in CSM calculations. c) A comparion of Δ_n^{csm} for even-N systems (solid symbols) with odd-even neutron mass differences, Δ_n^{oe} (open symbols). From ref. 13.

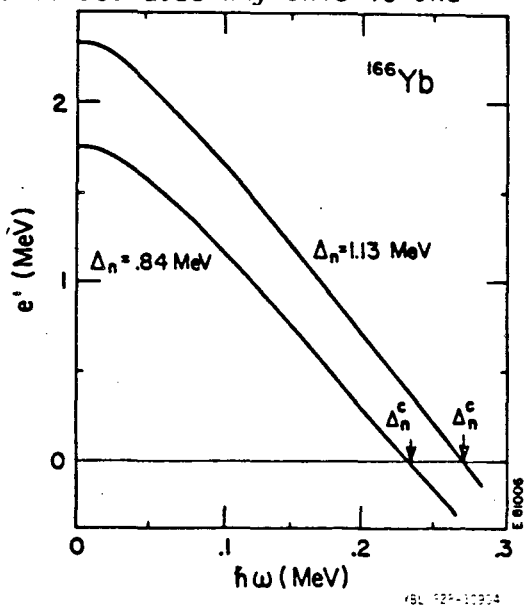

Fig. 10. Cranked shell-model two-quasineutron energies calculated as a function of $\hbar\omega$ for ^{166}Yb with ϵ_2 = 0.246 and ϵ_4 = 0.005 and two different values of Δ_n (0.84 and 1.13 MeV). The shift in $\hbar\omega_c$ corresponding to a change in Δ_n is indicated. From ref. 13.

case. Decreasing the gap (e.g. Δ_n = 0.84 MeV in Fig. 10) does not cause much change to the slope of a given orbital (aligned angular momentum), so that the crossing comes earlier (lower frequency). From calculations, one can estimate the gap necessary to produce the crossing frequencies shown in Fig. 9a. This calculated gap is shown in Fig. 9b (middle) for both the even and odd systems, and those from the even systems are compared with gaps from measured odd-even mass differences in Fig. 9c (top). Finally, in Fig. 11 the differences between the even- and odd-mass systems (solid points) are compared with those estimated from calculations (open points). The agreement is good, giving strong evidence that this technique is going to be a powerful one for studying pairing effects. Note that the change in gap can be measured for a specific configuration (band). Thus, still more detailed studies are possible looking at the small changes resulting from blocking different orbitals. Very recent results of this type have been interpreted as an effect of quadrupole pairing.

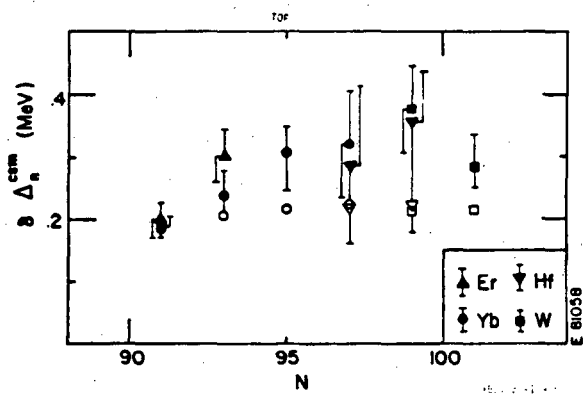

Fig. 11. The difference between Δ_n^{csm} (see fig. 9) for neighboring even- and odd-N isotopes (solid symbols) is compared with the calculated reduction in Δ_n (open symbols) due to the "blocking" of the negative-parity orbit nearest to the Fermi surface. From ref. 13.

CONCLUSION

Rotational frequency may thus be viewed as a "dimension" along which nuclear properties vary. This is an exciting development. There are other such "dimensions", for example, shape, temperature, deformation, etc., but they cannot be varied systematically (if at all). A rotational band, however, is simply a sequence of snapshots of a given configuration at progressively higher and higher rotational frequencies. The frequency can be varied right up to the point where the nucleus is disrupted by fission. Since there are distinguishable features, i.e., alignments, along these bands, one can study in great detail any nuclear property to which the alignments are sensitive.

PART 2

THE HIGHEST SPIN STATES

INTRODUCTION

In the first part of this report I discussed the rotational bands in deformed nuclei up to spin 30 ħ or so. There are very well-developed bands in this region that initially follow the simple rotational energy expression (Eqn. 1) quite closely. Nevertheless, large deviations from this simple collective behavior eventually develop, and I discussed those having to do with the collapse of the pairing correlations and the alignment of single-particle angular momenta. The conclusion was that these rotational bands offer a unique opportunity to study individual configurations as a function of a controlled variable, in this case, rotational frequency. In this second part of the report I want to address the question of what happens at still higher rotational frequencies—up to the highest angular momenta that nuclei can hold.

EXPECTED PROPERTIES OF HIGH SPIN NUCLEI

Maximum Angular Momentum

In practice there are some problems studying the very highest angular momentum states in nuclei. It is not even possible to specify the maximum angular momentum that a nucleus can hold without specifying a time scale. For example, a target and projectile nucleus may be in contact momentarily with as much as 500 ħ in the system. The way angular momentum is transferred into the internal degrees of freedom of the two nuclei is one of the fascinating aspects of reaction mechanism studies, but such a system cannot fuse and the angular momentum is largely returned to the external degrees of freedom as the system separates. In order to live longer than the collision time of $\sim 10^{-20}$ s, a system must have a nonvanishing barrier against fission, and the point at which this occurs can be readily estimated using the liquid-drop model (14). This model considers the nucleus as an incompressible fluid with volume, surface, Coulomb, and rotational (based on the equilibrium shape) energies. Its success in giving average nuclear properties under various conditions has been impressive from the earliest days of nuclear physics. The angular momentum for which the fission barrier vanishes has been calculated by Cohen et al. (15) and is shown as a function of mass number by the solid curve in Fig. 12. This represents the maximum angular momentum that a "cold" idealized nucleus could contain and is about 100 ħ for A ~ 130. It is lower for higher mass numbers because of the increasing Coulomb repulsion and for lower mass numbers because of the lower surface energy and the higher rotational

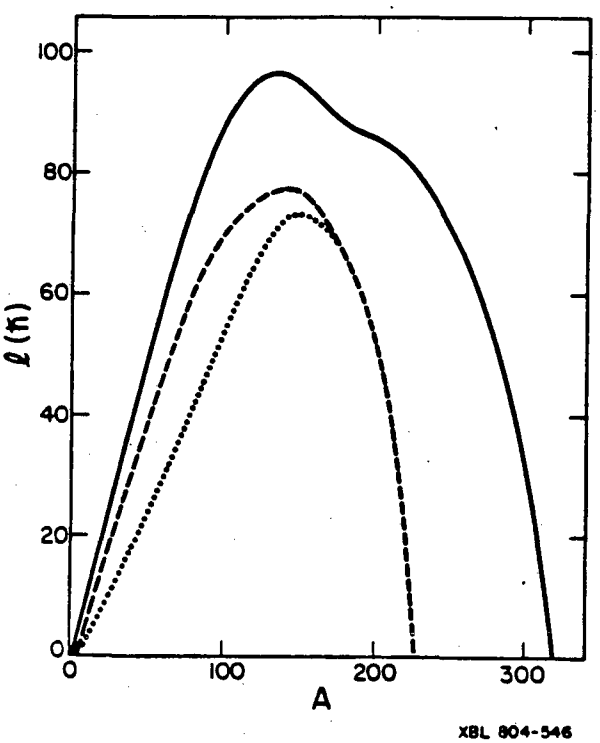

Fig. 12. The solid line indicates the angular momentum value for a given mass number A where the fission barrier just vanishes according to the liquid drop model, and the dashed line shows where it is about 8 MeV (ref. 15). The dotted line is an estimate of the boundary between particle evaporation (above) and γ-ray emission (below) estimated from experimental data.

frequencies required by the smaller moments of inertia. If cold nuclei could be produced at these angular momenta, spectroscopic studies might be possible up to this limit. But the heavy-ion fusion reactions that bring in this much angular momentum also bring in of order 40 MeV of excitation energy (or more), greatly increasing the fission probability. In order to prevent fission (where most of the angular momentum goes into the relative motion of the fragments), another process must de-excite the nucleus, and at such excitation energies this can only be particle evaporation. The time scale for this particle evaporation is 10^{-17}-10^{-18} s, and in order to slow the fission down to such times, a fission barrier of the order of the neutron binding energy (~8 MeV) is required. The dashed line in Fig. 12 corresponds to an 8-MeV fission barrier, below which particle evaporation should dominate. Between these lines, or in the time range 10^{-17}-10^{-21} s, essentially only fission of the system can be studied, and there is little information about nuclear structure in this region. When the decreasing level density slows the particle evaporation sufficiently (~10^{-15} s), or the excitation energy is below the neutron binding energy, γ-ray emission takes over and de-excites the nucleus to its ground state. The angular momentum removed by the particle evaporation is small if neutrons or protons are evaporated (~1 ħ per particle and only ~5 particles) but can be quite large (up to 20 ħ) for α particles. An estimate of the maximum angular momentum surviving the particle evaporation has been made based on γ-ray and α-particle emission probabilities and is shown as the dotted line in Fig. 12. Between the dashed and dotted lines (10^{-17}-10^{-15} s) the states can be studied by means of the evaporated particles, a method more sensitive to the nuclear structure than fission but much less sensitive than γ-ray decay. We want to consider only the γ-ray studies of high angular momentum states, which have access to the region below the dotted line in Fig. 12. It is easy to understand why these studies have centered first around the region A ~ 140, where spins up to ~70 ħ are accessible.

We are interested in the structure of nuclei at these high spins. Below about 30 ħ, where the population following these heavy-ion fusion reactions "condenses" into a few ($\lesssim$10) paths, one can resolve the de-excitation γ rays and make the kind of detailed spectroscopic studies described in Part 1 of this report. However, above ~30 ħ the population is spread over too many states and the γ-ray spectrum cannot at present be resolved. In studying the unresolved ("continuum") spectrum from these very high-spin states, the approach has necessarily been more general, involving shapes and moments of inertia.

Nuclear Shapes

At high spin the pairing correlations in nuclei are almost surely quenched, so we begin by considering the rigid rotation of shapes with quadrupole deformation: ellipsoids. The ratio of the moment of inertia $\mathcal{J}$ of a rigid ellipsoid of constant volume to that of a sphere, $\mathcal{J}_0$, is shown in Fig. 12 as a function of the shape parameter γ for two values of the deformation, ϵ. Values of $\gamma = 0^\circ$ and $\gamma = -120^\circ$ correspond to a prolate nucleus rotating perpendicular and parallel, respectively, to the symmetry axis; and $\gamma = -60^\circ$ and $\gamma = 60^\circ$ correspond to an oblate nucleus again rotating perpendicular and parallel to the symmetry axis, respectively. These axially symmetric limiting cases are shown by small figures in Fig. 13, and the regions between are triaxial shapes with all three axes of different length. It can be seen that shapes with $\gamma = 0^\circ$ to 60° have large (almost equivalent) moments of inertia and so should provide the lowest lying states for nuclei at these deformations. To translate this into energy terms, one must choose a particular nuclear mass and spin; an energy scale is shown on the right-hand ordinate for A = 160 and a spin of 60 ħ. The favored shapes are 10-15 MeV lower in energy than the unfavored ones. Since shell effects on the shape are usually

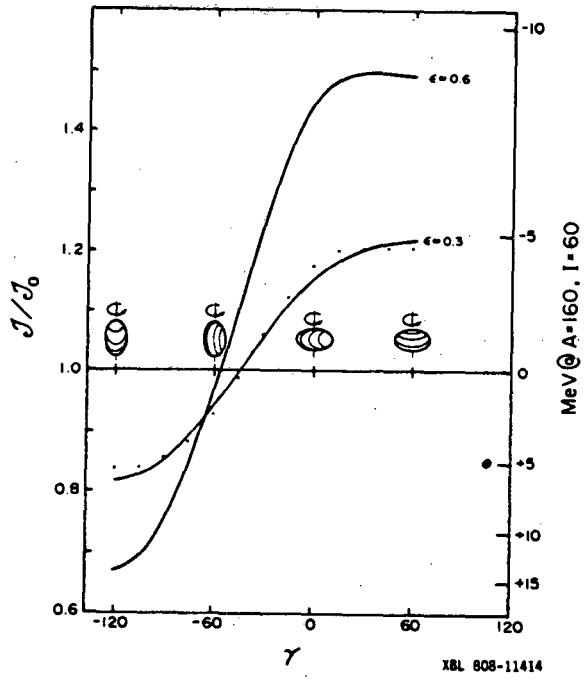

Fig. 13. The ratio of the moment of inertia of a rigid ellipsoid to that of a rigid sphere vs the shape parameter γ for two values of the deformation $\epsilon = 0.3$ and $\epsilon = 0.6$. The right-hand scale gives the difference in rotational energy in MeV for a nucleus with A = 160 and I = 60. The dots give the ratios for the total liquid-drop energy (rotation + surface + Coulomb) of the nucleus.

several times less than this, the favored moment-of-inertia region should dominate at high spins. The shape dependence of the surface and Coulomb energy terms in the liquid-drop model is small, so that the full liquid-drop model energy, given by the dots on Fig. 13, is a curve very near to that of the geometrical shape alone. Thus, at high spins simple geometry plays an important role in determining the nuclear shape (just as it does for the earth). A prolate nucleus rotating around an axis at right angles to the symmetry axis is just the system described by the rotational model (eqn. 1), with strongly enhanced E2 transitions connecting the levels. The other low-lying system, the oblate nucleus rotating around its symmetry axis, is not a collective motion; such a nucleus builds up angular momentum by the alignment of individual high-j nucleons along the rotational axis. A number of examples of such noncollective level schemes exist, particularly in the N = 82, Z = 64 region. There are now detailed model calculations of equilibrium shapes for many nuclei as a function of spin. Fig. 14 shows the prediction for several Er and Yb nuclei based on both Woods-Saxon and Nilsson potentials (16). All the calculated shapes in this region fall in the expected range as described above (except a few in the t_- regions), and there is, in general, very good agreement between the results from the different potentials. If the experimental results show as rich a variety of shapes as do these calculations, this field will be exciting in the next few years.

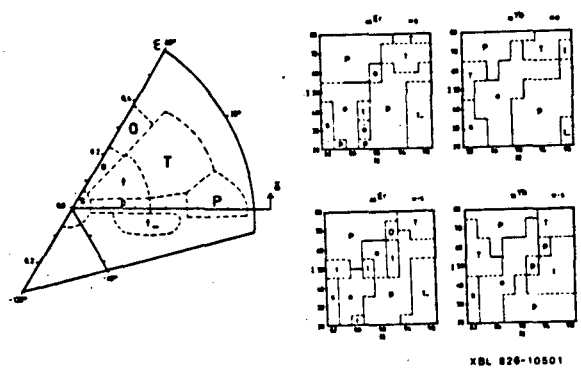

Fig. 14. The left side identifies various regions in a β-γ plot with appropriate symbols. The right side shows the shape (by symbol) calculated to be lowest in energy for Er and Yb nuclei as a function of spin and neutron number. Dashed boundaries indicate barriers less than 1 MeV between the regions; whereas, solid boundaries correspond to greater than 1 MeV barriers. Solutions for two potentials are shown--modified oscillator and Woods-Saxon. From ref. 16.

Moments of Inertia

As a consequence of the interplay between collective and single particle motions, there are a variety of moments of inertia one can measure and compare with detailed nuclear model calculations. The first distinction to make is between kinematic and dynamic values. Referring to Eqn. 1, one sees that a moment of inertia may be defined from the first derivative of the energy with respect to spin:

$$\frac{\mathcal{J}^{(1)}}{\hbar^2} = I\left(\frac{dE}{dI}\right)^{-1} = \frac{I}{\hbar\omega} \quad , \tag{4}$$

where $\mathcal{J}^{(1)}$ is called the "kinematic" moment of inertia because it has to do with the motion of the system--the ratio of angular momentum to angular frequency. It is also apparent that the second derivative leads to a definition:

$$\frac{\mathcal{J}^{(2)}}{\hbar^2} = \left(\frac{d^2E}{dI^2}\right)^{-1} = \frac{dI}{\hbar d\omega} \quad , \tag{5}$$

where $\mathcal{J}^{(2)}$ is called the "dynamic" moment of inertia since it has to do with the way the system will respond to a force. If there is only the kinetic energy term as given in Eqn. 1, these are equal; but, in general, when there are additional I-dependent terms in the Hamiltonian these two moments of inertia will differ. In the present case, the Coriolis force perturbs the internal nuclear structure, giving rise, in lowest order, to an (I j) term, so that $\mathcal{J}^{(1)} \neq \mathcal{J}^{(2)}$. This situation is not uncommon in other branches of physics. The arguments carry over into translational motion, where $p^2/2m$ is analogous to $I^2/2\mathcal{J}$, and additional momentum-dependent terms in the Hamiltonian give rise to two observed masses. Bohr and Mottelson have pointed out that an electron moving in a crystal lattice is a close analog, where the kinematic mass determines the level density and related statistical mechanical properties; whereas the response of the electron to an external force depends on a different, dynamic mass. In cases where the extra (angular) momentum-dependent term(s) depend on (I^2) p^2 (or so long as they can be expanded in lowest order as such) they can be taken together with the kinetic term to give a renormalized, "effective" (moment of inertia) mass.

These two moments of inertia can be defined in principle for any sequence of states desired, but certain ones occur rather naturally in the decay processes. So long as the particle configuration is frozen, so that one is confined to a band, the appropriate moments of inertia are $\mathcal{J}^{(1)}_{band}$ and $\mathcal{J}^{(2)}_{band}$. When there is no perturbation (alignment, shape change, etc.) of the internal structure along this band, these correspond to "collective" values. In general, however, a single decay pathway involves a sequence of bands having different alignments. Then the overall variation of spin with frequency is different and defines "effective" moments of inertia $\mathcal{J}^{(1)}_{eff}$ and $\mathcal{J}^{(2)}_{eff}$. These (especially $\mathcal{J}^{(2)}_{eff}$) have large variations in regions where a change of bands involves a large change in alignment (backbend or upbend). For the unresolved spectra from the highest spin states, the population is spread over many bands in many decay sequences. Nevertheless, the average band moments of inertia can be determined by looking for successive rotational transitions as correlations in γ-γ coincidence spectra. Similarly, the overall spin and γ-ray energies and their variations are also measurable giving the average effective moments of inertia. These will be discussed briefly, together with their comparison and interpretation.

EXPERIMENTAL DATA

A number of studies have been made over the last 10-15 years of the unresolved γ rays emitted from the highest spin states. It has been established that there are two types of γ rays emitted: statistical ones (3 or 4) that cool the nucleus to the yrast line and "yrast-like" ones ($\lesssim$30) that remove the angular momentum and contain most of the nuclear structure information. For some nuclei essentially

all the yrast-like transitions are collective rotational ones, and for most nuclei at least those from the very highest spin states are. In addition, systematic searches for noncollective behavior (as evidenced by the existence of isomers) have given negative results, generally above ~30 ħ, and in all cases surveyed above 40 ħ. Thus the methods developed to study the highest spin states center on ways to extract information from unresolved rotational sequences.

Measurement of $\mathcal{J}^{(2)}_{band}$

The γ-ray spectrum from a rotational nucleus is highly correlated in time, spatial distribution, and energy. For a perfect rotor, it is easy to show from eqn. 1:

$$E_\gamma = 2\,\frac{dE}{dI} = \frac{\hbar^2}{2\mathcal{J}}\,(4I_i - 2) \quad , \tag{6}$$

where I_i is the initial spin. This spectrum is composed of equally spaced lines, up to some maximum energy corresponding to the decay of the state with highest angular momentum, I_{max}. One aspect of the energy correlations is that no two γ rays have the same energy. If plotted on a two-dimensional diagram of $E_\gamma^{(1)}$ vs $E_\gamma^{(2)}$, such energies give a pattern with no points along the diagonal and a series of ridges parallel to it. The width of the "valley" W along the diagonal is determined by the difference between γ-ray energies and is thus related to the band moment of inertia,

$$W = 2\,\Delta E_\gamma = 4\,\frac{dE_\gamma}{dI} = 8\,\frac{d\omega}{dI} = \frac{8\,\hbar^2}{\mathcal{J}^{(2)}_{band}} \quad . \tag{7}$$

The important point is that the spectrum need not be resolved to determine the valley width. All that is required is that the populated bands have somewhat similar moments of inertia at a given frequency (γ-ray energy).

The data (17) in Fig. 15 come mainly from ^{161,160}Er nuclei formed by bombarding ^{124}Sn with ^{40}Ar at sufficient energy (185 MeV) to bring into the fused system all the angular momentum the nucleus can hold (~70 ħ). The data have been "symmetrized" around the diagonal in order to improve the statistics and have an "uncorrelated" background subtracted. A valley is clear up to energies ~1 MeV, and again probably from 1.1 to 1.2 MeV. Resolved lines have been seen in this case only up to ~0.8 MeV. The width of the valley in both the upper and lower region is about the same and can be evaluated to give $\mathcal{J}^{(2)}_{band}/\hbar^2 \approx 50\ \mathrm{MeV}^{-1}$, around two-thirds of the rigid-body value. Together with the effective moments of inertia, this is an important clue as to the nuclear structure in this region, as will be seen. In these correlation plots, the valley can be filled by irregularities in the bands, alignments, for example. These produce several transitions in the same energy region, and not only fill the valley but produce "stripes" of higher coincidence intensity at these γ-ray energies. It is important to appreciate that the alignments are expected to occur in many bands at nearly the same frequency. This happens when the "vacuum" defined in connection with Fig. 8 changes character; then all nonblocked configurations experience a band crossing and should generate a "stripe" even if the population is spread over many bands. So far rather little data of this type exist because the method is new and very demanding; one must have good statistics and complex but reliable analysis methods. Nevertheless, there is some evidence (18) for stripes at

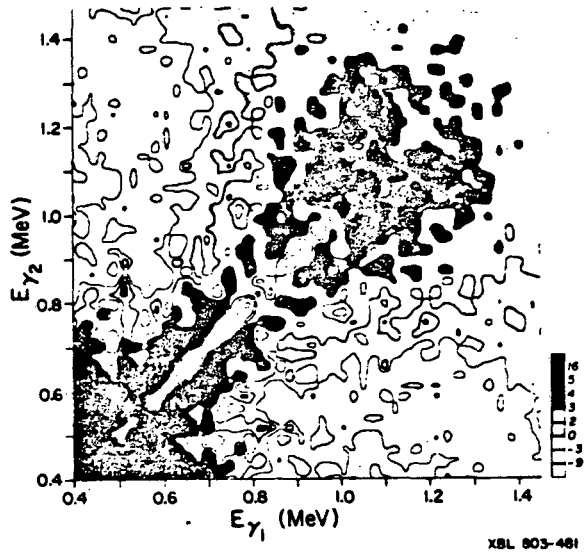

Fig. 15. Correlation spectrum from the reaction $^{124}Sn(^{40}Ar,xn)^{164-x}Er$ at 185 MeV. The data were taken on GeLi detectors and treated according to ref. 17. The plot shows contours of equal numbers of correlated events, where the darker regions have more counts according to the scale at the right edge.

frequencies up to at least ~0.6 MeV. If the spectra from the highest spin states cannot eventually be resolved, this will surely be one of the principal means for obtaining information about these states and, in particular, about band structures.

Measurement of $\mathcal{J}_{eff}$

The effective moments of inertia are simpler in some respects. They involve only relating a collective γ-ray energy with a spin or measuring the number of γ rays in an energy interval. The former gives $\mathcal{J}^{(1)}_{eff}$ values and has been measured several different ways, originally by relating the maximum γ-ray energy in a spectrum with the estimated maximum spin input (19). Recently, however, reliable methods for obtaining $\mathcal{J}^{(2)}_{eff}$ have been developed (20) and these are much more sensitive to the nuclear structure. If desired $\mathcal{J}^{(1)}_{eff}$ can then be obtained by integration. It is apparent that in a spectrum consisting only of "stretched" electric quadrupole ($I \rightarrow I-2$) transitions (which is known to be a good approximation in regions of rotational behavior), the number of transitions dN in a given γ-ray energy interval is just half the spin removed from that interval. If one knows the fraction of the observed population that goes through the interval, $f(E_\gamma)$, then (remembering $E_\gamma = 2\hbar\omega$):

$$\frac{H(E_\gamma)}{f(E_\gamma)} = \frac{dN}{dE_\gamma} = \frac{dI}{4\hbar\, d\omega} = \mathcal{J}^{(2)}_{eff}(\omega)/4\hbar^2.$$

The height of the spectrum $H(E_\gamma)$ gives directly $\mathcal{J}^{(2)}_{eff}(\omega)$. This was long recognized, but the difficulty was to find the feeding as a function of spin. Recently a method was developed using the spectra from two similar but slightly shifted spin distributions, whose difference is generally proportional to the feeding curve.

Figure 16 shows a spectrum of $^{159,160}Er$ resulting from the decay of a rather broad spin distribution centered at ~55 ħ. (This distribution is defined by selecting coincidences with a slice of the total γ-ray energy emitted by the nucleus. The total energy is detected in a large NaI crystal having an overall solid angle times efficiency of ~0.75 of 4π.) The statistical spectrum of γ rays, whose high-energy tail is seen above ~2 MeV, is subtracted leaving a spectrum of essentially pure collective transitions, and the $\mathcal{J}^{(2)}_{eff}$ values shown by the solid line in Fig. 17 result from correcting this for feeding (20). Two other cases, $^{161,162}Yb$ and $^{165,166}Yb$, are shown in Fig. 17. The general rise at low frequencies in all these nuclei is due to the quenching of the pairing correlations, and the irregularities below $\omega \approx 0.3$ MeV result from partially resolved individual γ-ray transitions and the known alignments (backbends), which cause several transitions to pile up at the same frequency. The band moments of inertia from the correlation data are plotted as lighter lines in the regions

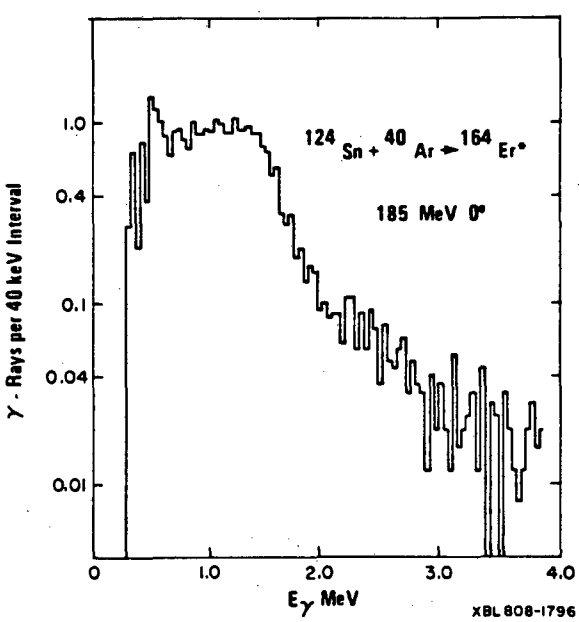

Fig. 16. Unresolved γ-ray spectrum for the indicated reaction taken with a NaI crystal and corrected for response function. The spectrum is that in coincidence with a slice of high-energy events (implying high spin) recorded in a large total-energy γ-ray detector. From ref. 19.

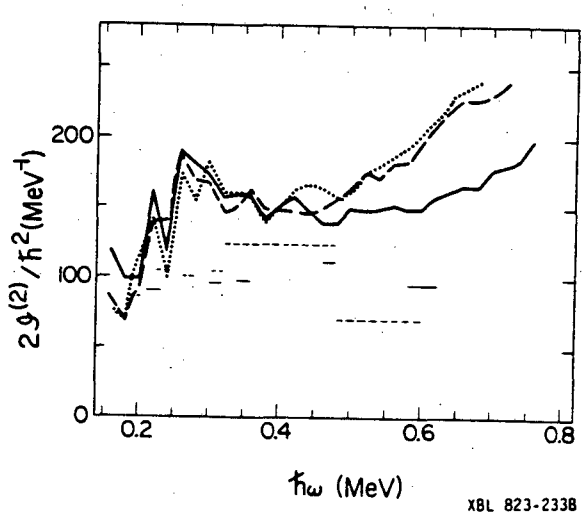

Fig. 17. $\mathcal{J}^{(2)}_{eff}$ as a function of $\hbar\omega$ for the systems $^{124}Sn + {}^{40}Ar$ (thick solid line), $^{126}Te + {}^{40}Ar$ (dotted line), $^{130}Te + {}^{40}Ar$ (thick dashed line). Also shown are some values of $\mathcal{J}^{(2)}_{band}$ for $^{124}Sn + {}^{40}Ar$ (thin solid lines) and $^{130}Te + {}^{40}Ar$ (thin dashed lines). From ref. 20.

where they have been determined. The rise in the effective moments of inertia above frequencies of 0.5 MeV seem to be associated with a drop in the band values. This suggests that alignments are becoming more important contributors of angular momentum. The higher values for the Yb (Z = 72) nuclei compared with ^{159,160}Er (Z = 70) suggests that protons play an important role here, which is in accord with calculations that predict proton $h_{9/2}$ and $i_{13/2}$ alignments in this frequency region.

SUMMARY

A schematic illustration of our current ideas about nuclear behavior as a function of frequency in the mass 160 region is shown in Fig. 18. This plot of I vs ω has vertical lines at the frequencies calculated for the major particle alignments, and there are two lines depicting moments of inertia corresponding to a rigid-body value and a value about half that large. The former corresponds to our expectation for $\mathcal{J}^{(1)}_{eff}$ of nuclei in general, and the latter is something like we might expect for the band moments of inertia, which are reduced first by pairing and then by the alignments. The heavy curve is the schematic path a nucleus might take, following the band values up except where alignments occur. This trajectory has the properties: 1) $\mathcal{J}^{(2)}_{band} = \hbar(dI/d\omega)_{band}$ is always half $\mathcal{J}_{rig}$; 2) $\mathcal{J}^{(1)}_{eff} = I\hbar/\omega$ is generally about equal to $\mathcal{J}_{rig}$; and 3) the $\mathcal{J}^{(2)}_{eff} = \hbar(dI/d\omega)$ is half $\mathcal{J}_{rig}$ except for large peaks at the alignments. The data are surprisingly similar: 1) $\mathcal{J}^{(2)}_{band}$ appears from rather fragmentary data to be between 1/2 and 2/3 of $\mathcal{J}_{rig}$; 2) $\mathcal{J}^{(1)}_{eff}$ is very

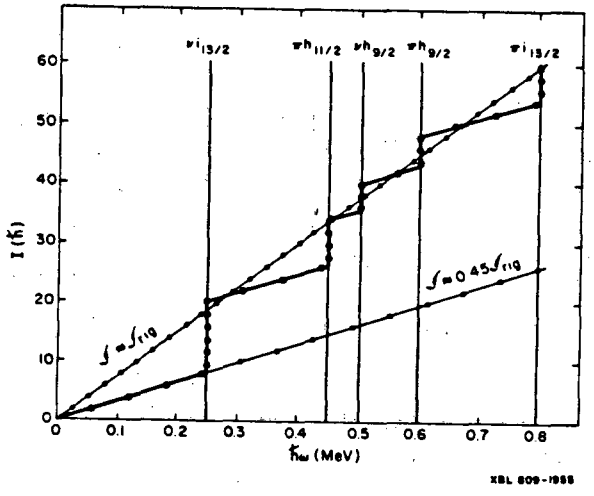

Fig. 18. Plot of spin vs rotational frequency ($E_\gamma/2$). The light lines show the trajectories of rotors having moments of inertia equal to (above) and 0.45 times (below) the rigid-body value. The vertical lines indicate the frequencies where the important high-j orbitals come near the Fermi level. The heavy line represents a trajectory for a realistic nucleus involving both rotation and alignment.

near $\mathcal{J}_{rig}$ except at low frequencies where the pairing correlation reduce it; and 3) $\mathcal{J}^{(2)}_{eff}$ behaves much as expected for frequencies below ~0.3 MeV. Above this point it is smooth and eventually rises, particularly in the Yb cases, far above $\mathcal{J}_{rig}$ over a rather long region. The smoothness indicates a smearing of the expected alignments. Whether the rise in $\mathcal{J}^{(2)}_{eff}$ is due to an alignment effect or signals some change in shape, or both, is not yet clear, though the proton $h_{9/2}$ and $i_{13/2}$ alignments could produce effects this large. Considering the alignments shown in Fig. 18, there is direct evidence for the first three in the resolved spectra of nuclei around mass 160. The first two have been experimentally identified as neutron $i_{13/2}$ and proton $h_{11/2}$, and the third has been suggested to be neutron $h_{9/2}$. Furthermore, there is evidence the next major alignments are due to protons. Altogether there is a remarkable agreement between the expectations and the facts, but a quantitative description of nuclear behavior at these highest spins is just beginning to emerge.

CONCLUSIONS

The study of high spin states is exciting, in part because the rotational frequency gives us a direction or dimension along which nuclear properties may be studied as was discussed in Part 1. Another interesting aspect is the question of what happens to the nucleus at very high frequency. The present, somewhat qualitative work shows that single particle alignment and collective rotation continue their competition to carry the angular momentum most efficiently. However, the recently measured $\mathcal{J}^{(2)}_{eff}$ values do not show the detailed structure expected at the highest frequencies. An interesting explanation could be that there are essentially no conserved quantum numbers at these frequencies, and all bands behave similarly. But this seems unlikely, both from theoretical grounds (see Fig. 7) and from the absence of highly correlated γ-ray spectra (well-developed valley-ridge structure) that should result. More likely the irregularities are washed out because the observed population is spread over many configurations and a broad temperature region. Restricting these population spreads should then reveal a wealth of detailed information.

There is great hope for the future in this area. A major experimental advance came with the advent of high resolution germanium (Ge) detectors about 15 years ago. These have recently become considerably larger, and furthermore subsidiary detectors to reject Compton scattered events are coming into use, giving unprecedented efficiency and response function to these detectors. Arrays of ~20 such detectors are being constructed and should provide the capabilities for identifying many more configurations at much higher frequencies. In parallel, two 4π sodium iodide detector arrays have been built, with 72 and 162 elements, that will detect every γ ray emitted in an event (though with lower energy resolution). This will make it possible to identify the spin and excitation energy of the initial state in a cascade. By selecting narrow regions of initial states, there is reasonable hope that the following cascades will be completely resolvable, up to the highest spins. Combinations of these two types of detector systems should provide a completely new generation of data on nuclei at high rotational frequencies. We should find answers for some of the questions we can just now begin to formulate.

PART 3

COLLECTIVE BANDS IN TRANSITIONAL NUCLEI

INTRODUCTION

In the first two parts of this report I have discussed the most collective band we know about in nuclei; namely, that based on the rotational degree of freedom. This degree of freedom is coupled to a number of others in the nucleus, the most obvious ones being the octupole vibrations and the low-lying $K = 0^+$ and $K = 2^+$ vibrations. In the case of the low-lying $K = 2^+$ vibration the coupling becomes so strong in some transitional nuclei that a two-band system results where the inter- and intra-band transitions are comparably enhanced. This general behavior has been known and studied for many years, but no simple, satisfying description of these states has yet been given. I want to discuss some recent measurement of E2 matrix elements in some Os and Pt nuclei. The objective is to compare these values with those from the IBA model and from the older "geometric" models.

A "dictionary" of the names I shall use is given in Fig. 19. There are four reasonably well-defined limiting situations in the geometric picture of quadrupole

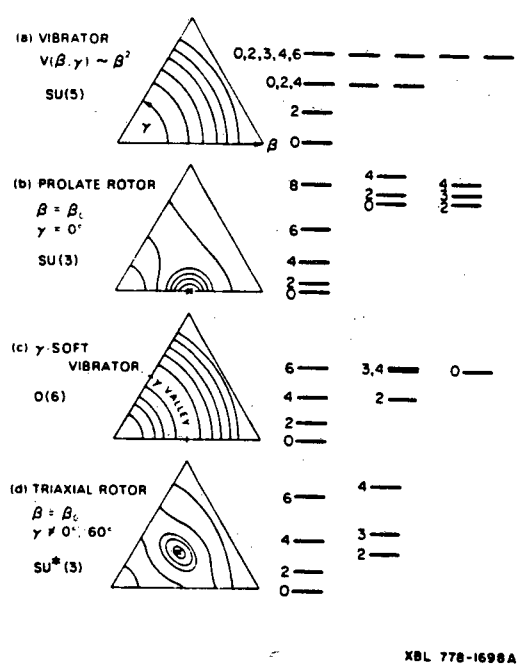

Fig. 19. The four characteristic types of spectra generated by simple potentials in the geometric model and by limiting symmetries in the IBA model.

oscillations in nuclei: the spherically symmetric vibrator (a); the prolate rotor (b); the γ-unstable vibrator (c); and the triaxial rotor (d). A corresponding limiting symmetry in the IBA model has been found for each of these cases, as indicated in Fig. 19, where the recently discovered SU*(3) analog to the triaxial rotor completes the scheme. The Pt and Os nuclei I want to discuss are not like the vibrator or prolate rotor (a or b in Fig. 19) but seem to have features resembling both the γ-unstable vibrator and the triaxial rotor (c and d). The differences between these two cases are not generally large, though some variation in the level positions within the $K = 2^+$ band occurs, and a second 0^+ level exists in the γ-unstable vibrator but not in the rigid triaxial rotor. The conclusions from the experimental level positions are ambiguous in regard to choosing between these models. Similarly, the IBA fits [all prior to the discovery of the SU*(3) symmetry] are not very convincing. The aim of the work reported here is to measure electromagnetic moments in these nuclei as a more sensitive test of the models. The questions are: (1) is there an adequate simple model; (2) if not, which is the best approximation and what kind of deviations occur.

METHOD

The philosophy of the present method is to study selectively those levels that have a relationship to the problem of interest. In this case, the Coulomb excitation process is ideal, in that it populates all states connected to the ground state by strong electric quadrupole (E2) transitions (except for occasional cancellations). This represents exactly the degree of freedom we want to explore. However, Fig. 20 shows the complexity of the problem. In this "typical" case there are ~10 each of (1) strong E2 transitions (solid arrows), (2) weak E2 transitions (dashed arrows or not drawn), and (3) diagonal E2 matrix elements.

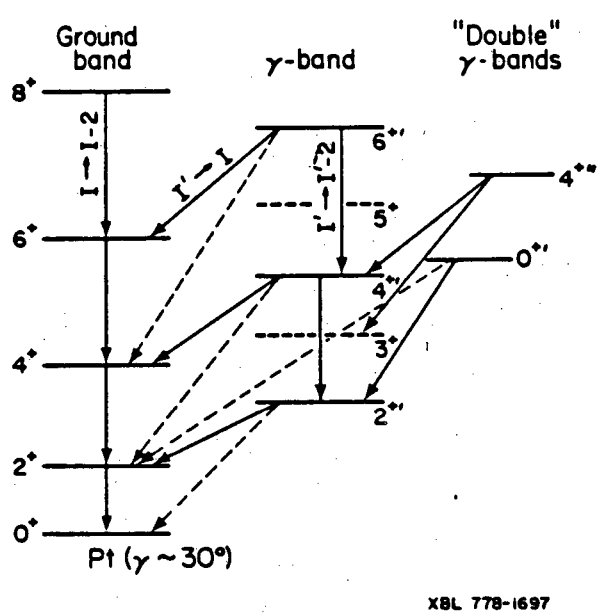

Fig. 20. Schematic level scheme and transitions for the Pt-Os type nuclei. The solid transitions have large matrix elements and the dashed transitions weaker ones. The dashed levels are not seen in Coulomb excitation due to a cancellation of amplitudes.

Thus, the Coulomb excitation of these levels depends on ~30 matrix elements. These can behave in rather complex ways; for example, population of the odd-spin members of the γ-band is systematically very low due to a cancellation of amplitudes from the two principal population routes. On the other hand, one can use many projectiles at several energies each to study a given target, so the problem clearly can be solved.

An additional advantage of the Coulomb excitation process is that it is most sensitive to the large matrix elements, so these can be best determined (about half or so of the ~30 total). These are much the best to compare with models, since they are less sensitive to small details in the model or to the small perturbations inevitably present. I shall discuss here only the larger matrix elements, significantly enhanced over the single-particle value, though two or three weak matrix elements involving low-lying levels are determined with reasonable accuracy.

An essential step in extracting matrix elements from the Coulomb excitation of a complex nucleus like this is the development of a computer program to fit many data points by variation of ~30 matrix elements. This has been done by Doug Cline and his co-workers (21) at Rochester, and I shall report some of the first results from such analyses. Doug has realized the need for many data points and the results for ^{194}Pt involve projectiles of ^{16}O, ^{40}Ca, ^{58}Ni, ^{136}Xe, and ^{108}Pb. Some 200 data points exist and can determine the 10 or 12 most sensitive matrix elements with good precision. The two Os cases I shall report are less extensive, involving ^{40}Ca, ^{58}Ni, and ^{136}Xe on ^{192}Os; and ^{58}Ni and ^{136}Xe on ^{190}Os. Our group at Berkeley has participated with Doug in taking the ^{136}Xe and ^{208}Pb data. The present report is preliminary and represents results from about two-thirds of the Pt and one-third of the Os data. The uncertainties were estimated using a sampling technique, where all matrix elements were varied according to random numbers within a given range.

RESULTS

The results are presented as plots against spin of (1) the strong transition matrix elements within and between the ground- and γ-bands and also that from the second 0^+ level and (2) the diagonal matrix elements in the ground- and γ-bands. Also on the plots are the results from several models: (1) the rigid asymmetric rotor (ARM), (2) the IBA model using the IBA2 parameters given in the paper by Bijker and colleagues (22), (3) the boson-expansion theory (BET) using computer ouptuts from Tamura (23), and (4) results (24) from either a γ-unstable model or one that is γ-soft (a rather shallow minimum in the potential for $\gamma \neq 0$). The results for each case are discussed separately below.

^{194}Pt

A spectrum of ^{194}Pt, Coulomb excited by Xe ions, is shown in Fig. 21 together with a partial level scheme. The presence of two strongly coupled bands is clear. The results for the E2 matrix elements of ^{194}Pt are shown in Fig. 22. I shall make only brief general comments, since more detail is probably not warranted at this stage. First, the ground-band transitions are not very sensitive to the model differences, but the BET and γ-unstable models are somewhat disfavored. The model transitions between the ground- and γ-bands fall into two groups—those with large dynamical variations in γ values and the ARM, which is rigid in γ. The data fall about midway between these groups. For transitions

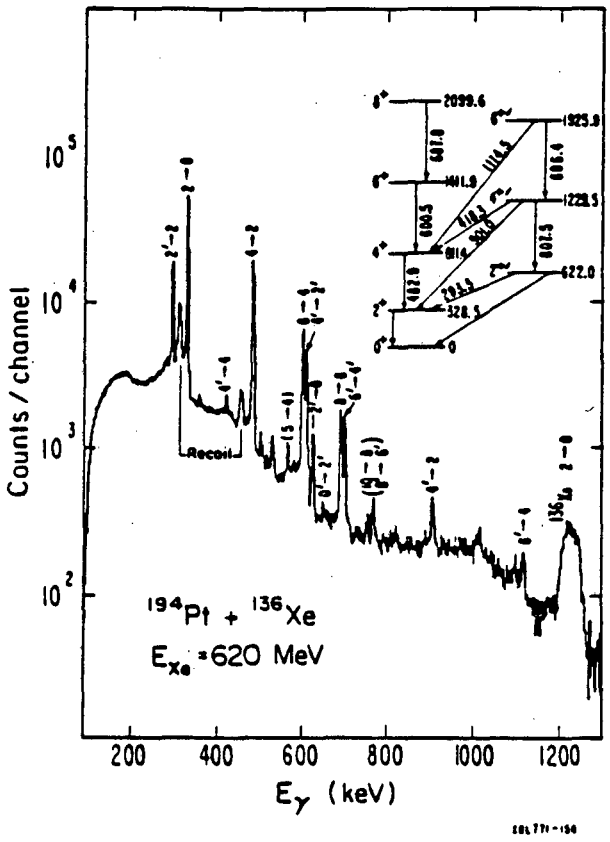

Fig. 21. Gamma-ray spectrum from ^{194}Pt Coulomb excited by ^{136}Xe ions.

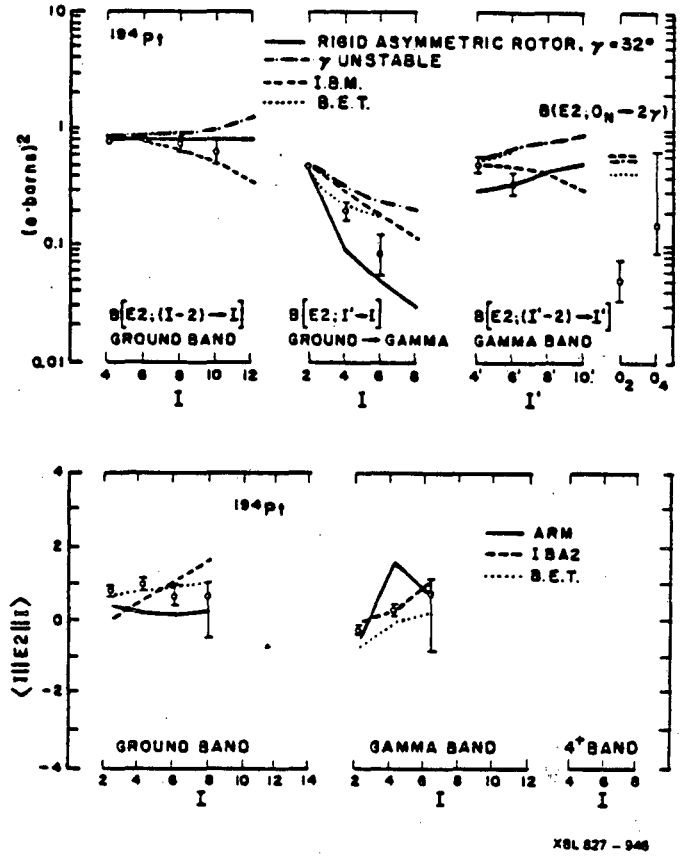

Fig. 22. Top. The B(E2) values measured for transitions in ^{194}Pt (ref. 21) compared with various models (see text). Bottom. The diagonal E2 matrix elements for ^{194}Pt (ref. 21) compared with various models.

within the γ-band, no model fits the data very well. The transition matrix element $0_2^+ \rightarrow 2_2^+$ is significant. It is far below the value of the variable-γ group defined above and yet clearly above zero—the γ-rigid value. The ground-band static moments are not very sensitive to the models, but the data do not show the steep trend given by the IBA model; rather, the best fit is given by BET. The γ-band static moments are also not so sensitive, but the high 4_2^+ value given by the ARM model seems not to occur in the data. Here the IBA gives the best fit. Overall, these ^{194}Pt data seem to call for models between the γ-rigid and γ-variable groups shown.

^{192}Os

For ^{192}Os, results in Fig. 23 are also shown from a calculation where a minimum in the value of γ occurred at 25° and was about 5 MeV deep. This should represent an intermediate situation between the γ-variable and γ-rigid models discussed above. The ground-band transitions are again not very sensitive to the models. The ground- to γ-band transitions are stronger here, favoring the γ-variable group of models rather than the ARM. The transitions within the γ-band are also not

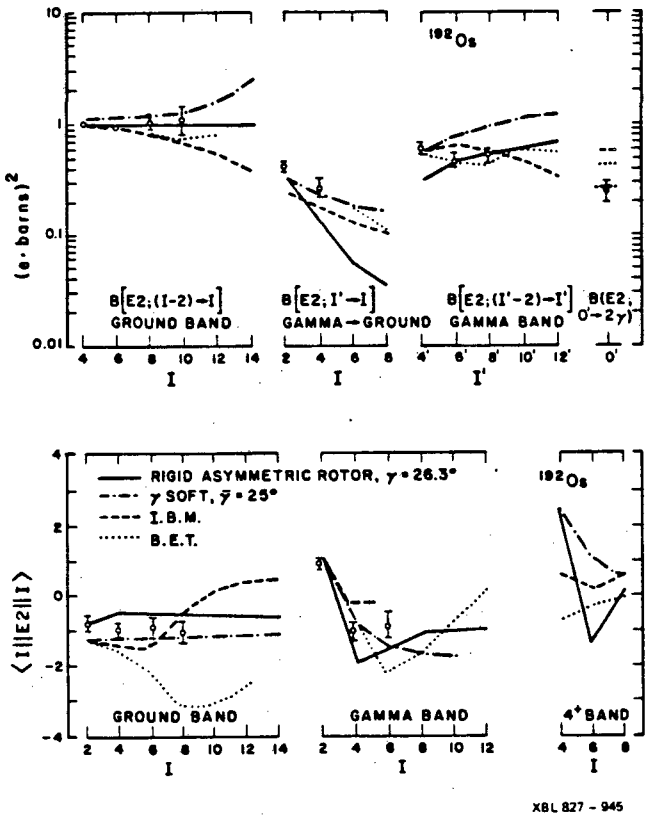

Fig. 23. As Fig. 22 except for ^{192}Os.

very sensitive to model but seem to disfavor the γ-soft model. The $0_2^+ \rightarrow 2_2^+$ transition is larger here, also indicating greater γ softness, and falls on the γ-soft model. The ground-band static moments are not so sensitive but do strongly disagree with the BET model. The behavior of the BET static moments is quite different from the rest, indicating some really different physics in this model (or perhaps an error in the code). The γ-band static moments are also not very sensitive to model but perhaps disfavor the more positive values of the IBA model. Overall, ^{192}Os is clearly softer in γ than ^{194}Pt. The γ-soft model, which should represent such physics, does very well except for the transitions within the γ-band, which are overpredicted. The reason for this is not clear.

^{190}Os

The nucleus ^{190}Os shown in Fig. 24 is moving toward the prolate rotor region as indicated by the larger static moments in both the ground- and γ-bands. The models differ rather little in their predictions for this nucleus, and only a few comments seem warranted. The $0_2^+ \rightarrow 2_2^+$ transition indicates less γ-softness than for ^{192}Os, as might be expected with increasing rotor characteristics. Also, the static moments of the BET model from the ground band seem too large (absolute value), and those of the IBA model for the γ-band slightly too positive.

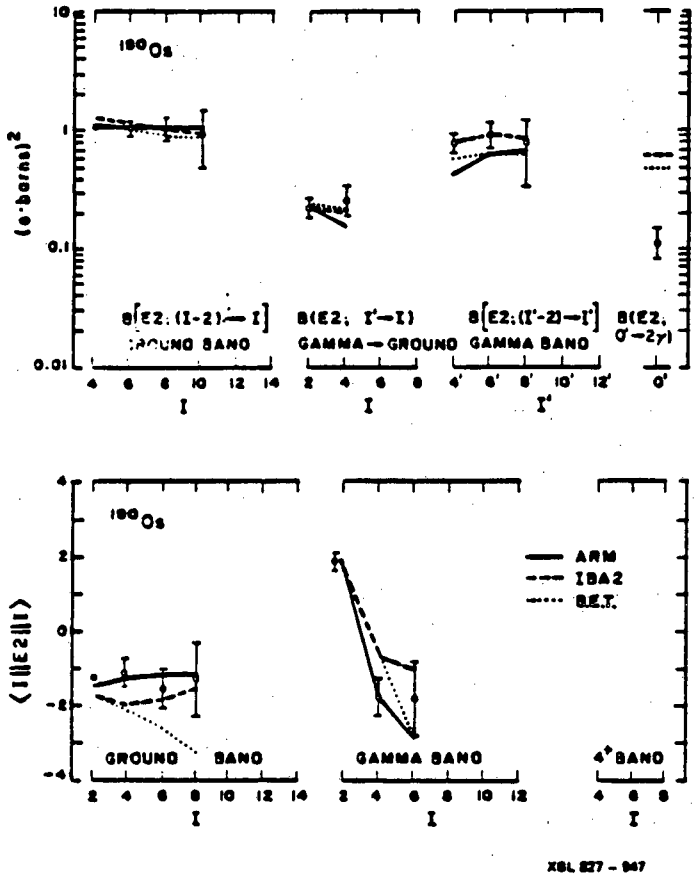

Fig. 24. As Fig. 22 except for ^{190}Os.

CONCLUSIONS

None of the simple models considered is adequate to explain the Pt and Os data on E2 moments reported here. The general physics, however, seems to be rather clearly indicated. One needs γ-soft models intermediate between the γ-rigid (ARM) and the γ-variable (BET, IBA, and γ-unstable) models considered here. The rigidity needed seems larger than is currently expected from the microscopic calculations. The IBA model seems comparable with the other γ-variable models. If the SU*(3) symmetry indeed offers a way to get more "rigidity effects" into this model, then it seems likely that situations between O(6) and SU*(3) will also give better fits to the data. It is not clear at this point whether there are basic differences in the results of the IBA and geometric models. Perhaps when better fits are obtained with intermediate "γ-soft type" models, it will be possible to distinguish between these general approaches.

REFERENCES

1. Bohr, A. (1952). Mat. Fys. Medd. Dan. Vid. Selsk., 26, no. 14.
2. Grosse, E., H. Balanda, H. Emling, F. Folkmann, P. Fuchs, R.B. Piercey, D. Schwalm, R.S. Simon, H.J. Wollerscheim, D. Evers, and H. Ower (1981). Physica Scripta, 24, 337.
3. Bardeen, J., L.N. Cooper, J.R. Schriefer (1957). Phys. Rev., 106, 162.
4. Johnson, A., H. Ryde, J. Sztarkier (1971). Phys. Lett., 34B, 605.
5. Stephens, F.S., and R.S. Simon (1972). Nucl. Phys., A183, 257.
6. Burde, J., E.L. Dines, S. Shih, R.M. Diamond, J.E. Draper, K.H. Lindenberger, C. Schuck, and F.S. Stephens (1982). Phys. Rev. Lett., 48, 530.
7. Herskind, B. (1980). J. de Physique, 41, C10-106.
8. Nilsson, S.G. (1955). Mat. Fys. Medd. Dan. Vid. Selsk., 29, no. 16.
9. Neergaard, K., H. Toki, M. Ploszajczak, and A. Faessler (1977). Nucl. Phys., A287, 48.
10. Mang, H.J. (1975). Phys. Rep., 18, 325;
    Faessler, A., K.R.S. Devi, F. Grummer, K.W. Schmid, and R.R. Hilton (1976). Nucl. Phys., A256, 106;
    Goodman, A.L. (1979). Adv. Nucl. Phys., 11, 263.
11. Andersson, C.G., S.E. Larsson, G. Leander, P. Moller, S.G. Nilsson, I. Ragnarsson, S. Aberg, R. Bengtsson, J. Dudek, B. Nerlo-Pomorska, K. Pomorski, and Z. Szymanski (1976). Nucl. Phys., A268, 205.
12. Hamamoto, I. (1981). Nordita preprint 81/28.
13. Garrett, J.D., and J.J. Gaardhoje (1980). XIV Masurian Summer School on Nuclear Physics, Mikolajki, Poland.
14. Bohr, N., and F. Kalckar (1937). Mat. Fys. Medd. Dan. Vid. Selsk., 14, no. 10.
15. Cohen, S., F. Plasil, and W.J. Swiatecki (1974). Ann. Phys., 82, 557.
16. Andersson, C.G., R. Bengtsson, T. Bengtsson, J. Krumlinde, G. Leander, K. Neergaard, P. Olanders, J.A. Pinston, I. Ragnarsson, Z. Szymanski, and S. Aberg (1981). Physica Scripta, 24, 266.
17. Deleplanque, M.A., F.S. Stephens, O. Andersen, C. Ellegaard, J.D. Garrett, B. Herskind, D. Fossan, M. Neiman, C. Roulet, D.C. Hillis, H. Kluge, R.M. Diamond, and R.S. Simon (1980). Phys. Rev. Lett., 45, 172.
18. Ellegaard, C., M.A. Deleplanque, O. Andersen, B. Herskind, F.S. Stephens, R.M. Diamond, H. Kluge, C. Schuck, S. Shih, and J.E. Draper (1982). Phys. Rev. Lett., 48, 670.
19. Simon, R.S., M.V. Banaschik, R.M. Diamond, J.O. Newton, and F.S. Stephens (1977). Nucl. PHys., A290, 253.
20. Deleplanque, M.A., H.J. Körner, H. Kluge, A.O. Macchiavelli, N. Bendjaballah, R.M. Diamond, and F.S. Stephens, submitted to Phys. Rev. Lett.
21. Cline, D., C.Y. Wu, T. Czosnyka, L. Hasselgren, P. Russo, J.K. Sprinkle, I.Y. Lee, P.A. Butter, R.M. Diamond, F.S. Stephens, C. Baktosh, S. Steadman, H. Kluge, G. Dracoulis, J. Leigh, J.O. Newton, W.R. Phillips, and S. Sie (1982). unpublished data.
22. R. Bijker, A.E.L. Dieperink, O. Scholten, and R. Spanhoff (1980). Nucl. Phys., A344, 207.
23. Weeks, K.J., and T. Tamura (1980). Phys. Rev., C22, 1323.
24. G. Leander (1976). private communication.

This work was supported by the Director, Office of Energy Research, Division of Nuclear Physics of the Office of High Energy and Nuclear Physics of the U.S. Department of Energy under Contract DE-AC03-76SF00098.

This report was done with support from the Department of Energy. Any conclusions or opinions expressed in this report represent solely those of the author(s) and not necessarily those of The Regents of the University of California, the Lawrence Berkeley Laboratory or the Department of Energy.

Reference to a company or product name does not imply approval or recommendation of the product by the University of California or the U.S. Department of Energy to the exclusion of others that may be suitable.

TECHNICAL INFORMATION DEPARTMENT
LAWRENCE BERKELEY LABORATORY
UNIVERSITY OF CALIFORNIA
BERKELEY, CALIFORNIA 94720